A&A 575, A85 (2015)
DOI: 10.1051/0004-6361/201323042

Astronomy & Astrophysics

Improved parameters of seven *Kepler* giant companions characterized with SOPHIE and HARPS-N⋆

A. S. Bonomo[1], A. Sozzetti[1], A. Santerne[2], M. Deleuil[3], J.-M. Almenara[3], G. Bruno[3], R. F. Díaz[4], G. Hébrard[5,6], and C. Moutou[3]

[1] INAF–Osservatorio Astrofisico di Torino, via Osservatorio 20, 10025 Pino Torinese, Italy
e-mail: bonomo@oato.inaf.it
[2] Instituto de Astrofísica e Ciências do Espaço, Universidade do Porto, CAUP, Rua das Estrelas, 4150-762 Porto, Portugal
[3] Aix Marseille Université, CNRS, LAM (Laboratoire d'Astrophysique de Marseille) UMR 7326, 13388 Marseille, France
[4] Observatoire Astronomique de l'Université de Genève, 51 chemin des Maillettes, 1290 Versoix, Switzerland
[5] Observatoire de Haute-Provence, Université Aix-Marseille & CNRS, 04870 St. Michel l'Observatoire, France
[6] Institut d'Astrophysique de Paris, UMR7095 CNRS, Université Pierre & Marie Curie, 98bis boulevard Arago, 75014 Paris, France

Received 13 November 2013 / Accepted 2 January 2015

ABSTRACT

Radial-velocity observations of *Kepler* candidates obtained with the SOPHIE and HARPS-N spectrographs have permitted unveiling the nature of the five giant planets Kepler-41b, Kepler-43b, Kepler-44b, Kepler-74b, and Kepler-75b, the massive companion Kepler-39b, and the brown dwarf KOI-205b. These companions were previously characterized with long-cadence (LC) *Kepler* data. Here we aim at refining the parameters of these transiting systems by i) modelling the published radial velocities and *Kepler* short-cadence (SC) data that provide a much better sampling of the transits; ii) performing new spectral analyses of the SOPHIE and ESPaDOnS spectra, after improving our procedure for selecting and co-adding the SOPHIE spectra of faint stars ($K_p \gtrsim 14$); and iii) improving stellar rotation periods hence stellar age estimates through gyrochronology, when possible, by using all the available LC data up to quarter Q17. Posterior distributions of the system parameters were derived with a differential evolution Markov chain Monte Carlo approach. Our main results are as follows: a) Kepler-41b is significantly larger and less dense than previously found because a lower orbital inclination is favoured by SC data. This also affects the determination of the geometric albedo that is lower than previously derived: $A_g < 0.135$; b) Kepler-44b is moderately smaller and denser than reported in the discovery paper, as a consequence of the slightly shorter transit duration found with SC data; c) good agreement was achieved with published Kepler-43, Kepler-75, and KOI-205 system parameters, although the host stars Kepler-75 and KOI-205 were found to be slightly richer in metals and hotter, respectively; d) the previously reported non-zero eccentricities of Kepler-39b and Kepler-74b might be spurious. If their orbits were circular, the two companions would be smaller and denser than in the eccentric case. The radius of Kepler-39b is still larger than predicted by theoretical isochrones. Its parent star is hotter and richer in metals than previously determined.

Key words. planetary systems – stars: fundamental parameters – techniques: photometric – techniques: spectroscopic – techniques: radial velocities

1. Introduction

Thanks to unprecedented photometric precision and temporal coverage, the *Kepler* space telescope has discovered over two thousand small-sized planetary candidates with radii $R_p < 4\ R_\oplus$ (Burke et al. 2014). At the same time, it has provided the exoplanet community with more than two hundred Jupiter-sized candidates, thus triggering further studies on the structure, formation, and evolution of giant companions as well as on their atmosphere, if the optical and/or near-infrared occultations are observed.

Since 2010 we have been following up several *Kepler* giant candidates orbiting faint stars with *Kepler* magnitudes $K_p \gtrsim 14$ using the SOPHIE spectrograph at the Observatoire de Haute-Provence (France). In addition to determining the fraction of false positives among the *Kepler* giant candidates (Santerne et al. 2012), this intensive follow-up allowed us to characterize the giant planets Kepler-41b/KOI-196b (Santerne et al. 2011a), Kepler-43b/KOI-135b and Kepler-44b/KOI-204b (Bonomo et al. 2012a), Kepler-74b/KOI-200b and Kepler-75b/KOI-889b (Hébrard et al. 2013); the massive companion Kepler-39b/KOI-423b in the brown-dwarf desert (Bouchy et al. 2011), which could be either an extremely massive planet or a low-mass brown dwarf; and the brown dwarf KOI-205b (Díaz et al. 2013). For two planets, that is for Kepler-74b and Kepler-75b, additional radial-velocity measurements were taken with the HARPS-N spectrograph (Cosentino et al. 2012), which has been installed at the Telescopio Nazionale *Galileo* at La Palma island in April 2012 (see Hébrard et al. 2013).

All these giant companions were characterized using *Kepler* data with long-cadence (LC) temporal sampling of 29.42 min, usually because short-cadence (SC) photometric measurements, that is one point every 58 s, were not available at the moment of publication. However, the long-cadence sampling presents the strong inconvenience of distorting the transit shape. This effect leads to longer transit durations, more V-shaped transits, hence lower ratios between the semi-major axis and the stellar radius than the true ones. This yields lower stellar densities from the Kepler's third law and thus makes both stellar and planetary radii appear larger than they actually are (Kipping 2010).

⋆ Tables 2–8 are available in electronic form at http://www.aanda.org

Table 1. IDs and *Kepler* magnitudes of the planet-hosting stars Kepler-39, Kepler-41, Kepler-43, Kepler-44, Kepler-74, Kepler-75, and KOI-205.

Kepler name	Kepler-39	Kepler-41	Kepler-43	Kepler-44
Object	KOI-423	KOI-196	KOI-135	KOI-204
Kepler ID	9478990	9410930	9818381	9305831
2MASS ID	19475046+4602034	19380317+4558539	19005780+4640057	20002456+4545437
Kepler magnitude K_p	14.33	14.46	13.96	14.68

Kepler name	Kepler-74	Kepler-75	–
Object	KOI-200	KOI-889	KOI-205
Kepler ID	6046540	757450	7046804
2MASS ID	19322220+4121198	19243302+3634385	19415919+4232163
Kepler magnitude K_p	14.41	15.26	14.52

To overcome this problem, Kipping (2010) suggested to perform the transit fitting by oversampling the transit model and then binning the model samples to those of the LC before computing the chi-square or the likelihood function. His Eq. (40) suggests a simple way to choose the resampling resolution, given the photometric precision of the light curve. Following this prescription, Kipping & Bakos (2011) analysed the LC data of Kepler-4b through Kepler-8b using a bin number of 4.

When modelling the transits of the *Kepler* planets observed with SOPHIE and HARPS-N, we therefore followed this suggestion by Kipping (2010) and oversampled the transit model by a factor five, which is higher than recommended by his Eq. (40). However, in some cases, the analysis of short-cadence data is mandatory especially when the orbital period is close to an integer multiple of the LC sampling $\delta T_{\rm lc}$ because this prevents the transit from being well sampled in orbital phase. The most evident case is Kepler-43b, whose orbital period is $P = 147.99 \cdot \delta T_{\rm lc}$ (see Fig. 5 in Bonomo et al. 2012a). In addition, the massive companion Kepler-39b did not present an optimal coverage of the transit ingress and egress in the quarters Q1 and Q2 that were analysed by Bouchy et al. (2011) because $P = 1032.14 \cdot \delta T_{\rm lc}$ (see Fig. 9 in Bouchy et al. 2011).

Moreover, by performing an homogeneous analysis of transit photometry from space and oversampling the *Kepler* LC data by a factor of ten instead of five, Southworth (2012) derived smaller stellar and planetary radii for some of the aforementioned giant companions, although his results agree with ours within 2σ. This would indicate that an oversampling of the transit model by a factor of five might not be ideal in all cases, hence an independent analysis of SC data is certainly recommended. Nevertheless, some of the slightly different results obtained by Southworth (2012) are also due to a better ephemeris and transit signal-to-noise ratio (S/N) because, in most cases, he used longer temporal series than we did, up to quarter Q6.

In this paper, we report the results of our analysis of the *Kepler* SC data of Kepler-39, Kepler-41, Kepler-43, Kepler-44, Kepler-74, Kepler-75, and KOI-205, along with the previously published radial velocities (RV). *Kepler* LC data up to quarter Q17 were used to refine stellar rotation periods by means of both generalised Lomb-Scargle periodograms (Zechmeister & Kürster 2009) and autocorrelation functions, when an unambiguous peak with FAP < 0.01% could be identified. This allows us to estimate system ages through gyrochronology (Mamajek & Hillenbrand 2008), after deriving the $B - V$ index colour and its uncertainty from Eq. (3) in Sekiguchi & Fukugita (2000). The IDs and *Kepler* magnitudes of the parent stars are listed in Table 1. This work aims at refining the characterization of these systems and possibly clarifying the apparently unusual properties of Kepler-39b and Kepler-41b. Indeed, the former was found to have a larger radius than predicted by theoretical isochrones of Baraffe et al. (2003), and Bouchy et al. (2011) were unable to find any reasonable explanation for this behaviour. The latter seemed to be a non-inflated planet despite its proximity to the host star, and to occupy an atypical position in the radius-mass and radius-$T_{\rm eq}$ diagrams of giant planets (see Figs. 9 and 10 in Santerne et al. 2011a).

Moreover, we performed new spectral analyses of the planet-hosting stars after improving our procedure of selecting, treating, and co-adding the SOPHIE spectra. A revision of the atmospheric parameters may have a significant impact on stellar, hence planetary, parameters.

We recognize the merit of an approach to revisiting stellar *or* planetary parameters of transiting systems that encompasses much larger samples (e.g., Torres et al. 2012; Southworth 2012) than the one presented here. Our work differs in that it performs a self-consistent re-analysis taking into account both photometric *and* spectroscopic measurements and constraints within a coherent Bayesian framework to derive the posterior density distributions of the full set of system parameters.

2. Data

2.1. Kepler photometry

Short-cadence measurements obtained with the simple-aperture-photometry pipeline[1] (Jenkins et al. 2010) were downloaded from the MAST archive[2]. Eleven quarters of SC data (Q3-Q7 and Q10-Q15) are available for Kepler-43; six quarters (Q10-Q15) for Kepler-75; four quarters (Q4-Q7) for Kepler-41, Kepler-44, Kepler-74, and KOI-205; and three quarters (Q12-Q14) for Kepler-39.

The medians of the errors of SC measurements of Kepler-39, Kepler-41, Kepler-43, Kepler-44, Kepler-74, Kepler-75 and KOI-205 are 1.20×10^{-3}, 1.27×10^{-3}, 8.9×10^{-4}, 2.02×10^{-3}, 1.24×10^{-3}, 3.26×10^{-3}, and 1.28×10^{-3} in units of relative flux, respectively.

For all targets, the flux excess originating from background stars that are located within the *Kepler* photometric mask was subtracted separately for each quarter by using the estimates provided by the *Kepler* team[3]. Indeed, this contamination of the

[1] http://keplergo.arc.nasa.gov/PyKEprimerLCs.shtmlp

[2] http://archive.stsci.edu/kepler/data_search/search.php

[3] http://archive.stsci.edu/kepler/kepler_fov/search.php; for Season 2 data of KOI-205, the value of crowding factor as derived by Díaz et al. (2013) was used (see Díaz et al. 2013).

target flux dilutes the transits, making them appear shallower than they are, even though it usually does not exceed 5–7% of the total collected flux.

All the SC data were used to model the transits of the seven giant companions. The signal-to-noise ratios of the phase-folded transits are of at least ~450 and, in some cases, higher than 1000. Thanks to these high S/N, we were able to derive stellar and planetary radii with uncertainties $\lesssim$3% almost in all cases (see Tables 2–8). At this level of precision, errors on planetary radii are dominated by the uncertainties on stellar models (Southworth 2011, 2012) and/or on the orbital eccentricity e and argument of periastron ω. Indeed, the uncertainties on e and ω from RV observations propagate into the transit parameter $a/R_\star$ and thus into the stellar density from the Kepler's third law. Stellar density is then used as a proxy for luminosity to determine stellar hence planetary parameters (e.g., Sozzetti et al. 2007) when no constraints from asteroseismology are available. This means that in our particular cases the additional use of LC data practically does not yield any significant improvement on planetary parameters while introducing possible covariances between transit parameters (Price & Rogers 2014). For this reason, as mentioned before, we used LC data only to derive stellar rotation periods.

2.2. Radial-velocity data

The RV observations considered in this work are those listed in the announcement papers because no additional observations with either SOPHIE or HARPS-N were carried out for these targets. The SOPHIE measurements were performed in high-efficiency mode with a resolution of ~40 000, and exposure times not exceeding 1 h. The observations of KOI-200 and KOI-889 carried out with HARPS-N were taken in high-resolution mode (the only available one) with a resolving power of ~110 000 and exposures of 45 min and shorter than 25 min, respectively. Both SOPHIE and HARPS-N measurements were performed in obj_AB observing mode with fibre A centred on the target and fibre B on the sky. When needed, the observations were corrected for moonlight pollution, as described in Bonomo et al. (2010).

2.3. Spectra

The atmospheric parameters of the host stars, along with the stellar density derived from the transit fitting, are of fundamental importance for determining stellar, hence planetary, parameters (Sozzetti et al. 2007).

While radial-velocity measurements can accommodate low S/N spectra, spectral analysis is more challenging. Indeed, some diffuse light in the SOPHIE spectrograph might affect the spectra at very low S/N acquired in high-efficiency mode. For this reason, we recently improved our procedure of treating and selecting the SOPHIE spectra to determine stellar atmospheric parameters. In particular, spectra with an S/N lower than 14 were excluded from the co-addition. Those acquired in the presence of the Moon were corrected for the moonlight contamination by subtracting the background as estimated from fibre B. As is usually done, the individual exposures were then set in the rest frame and co-added in a single master spectrum.

In the case of Kepler-39, the co-added spectrum obtained this way shows deeper lines than simply co-adding all the SOPHIE spectra, as was previously done by Bouchy et al. (2011). This has a significant impact on the derivation of the atmospheric parameters (see Sect. 4.1).

The S/N of the SOPHIE master spectra at 600 nm and per element of resolution ranges between 100 and 170 for Kepler-39, Kepler-41, Kepler-43, Kepler-44, and Kepler-74. It is equal to 72 and 65 for KOI-205 and Kepler-75, respectively.

Two host stars, namely KOI-205 and Kepler-39, were also observed with ESPaDOnS at the 3.6-m Canada-France-Hawaii Telescope in Mauna Kea as part of a programme dedicated to the characterization of *Kepler* planet-hosting stars[4]. The objective is indeed to carry out a better spectral analysis of the parent stars with a spectrograph that offers both a higher spectral resolution ($R \simeq 65\,000$) and an extended spectral coverage (370–1000 nm). These two targets were observed in "object+sky" mode. The ESPaDOnS spectrum of KOI-205 with a $S/N \sim 90$ was previously used by Díaz et al. (2013) to determine the host star and brown dwarf parameters. Kepler-39 was observed with ESPaDOnS on September 28, 2012 and December 1, 2012, in a series of five exposures of ~40 min. The individual spectra as reduced by the CFHT Upena/Libre-Esprit pipeline were co-added after they were set in the rest frame and resulted in a master spectrum with S/N of 65 in the continuum at 600 nm per resolution element. This co-added spectrum is analysed here for the first time.

3. Data analysis

3.1. Spectral analysis

To determine the effective temperature ($T_{\rm eff}$), surface gravity ($\log g$), and iron abundance [Fe/H], the co-added SOPHIE spectra obtained with our improved selection and those acquired with ESPaDOnS were reanalysed following the same procedures described in detail by Sozzetti et al. (2004, 2006) and references therein. A set of ~60 relatively weak lines of Fe I and 10 of Fe II were selected, and EWs were measured using the TAME software (Kang & Lee 2012). Metal abundances were derived assuming local thermodynamic equilibrium (LTE), using the 2010 version of the spectral synthesis code MOOG (Sneden 1973), a grid of Kurucz ATLAS plane-parallel model stellar atmospheres (Kurucz 1993), and imposing excitation and ionisation equilibrium. Uncertainties in the parameters were estimated following the prescriptions of Neuforge & Magain (1997) and Gonzalez & Vanture (1998) and rounded to 25 K in $T_{\rm eff}$ and 0.05 dex in $\log g$.

The derived atmospheric parameters are compared in Sect. 4.1 with the literature values, which were obtained with i) the iterative spectral synthesis package VWA (Bruntt et al. 2010) for Kepler-39, Kepler-41, Kepler-74, Kepler-75, and KOI-205; and ii) the 2002 version of the MOOG code with the methodology described in Bonomo et al. (2012a) and Mortier et al. (2013) for Kepler-43 and Kepler-44.

3.2. Combined analysis of Kepler and radial-velocity data

To derive system parameters, a Bayesian analysis of *Kepler* SC photometry and RV measurements was performed, using a differential evolution Markov chain Monte Carlo (DE-MCMC) method (Ter Braak 2006; Eastman et al. 2013). For this purpose, the epochs of the SOPHIE and HARPS-N observations were converted from $\mathrm{BJD_{UTC}}$ into $\mathrm{BJD_{TDB}}$ (Eastman et al. 2010), which is the time stamp of *Kepler* data.

The transit fitting was performed using the model of Giménez (2006, 2009). For this purpose, each transit was normalised by locally fitting a slope to the light-curve intervals of

[4] Programme 12BF24, PI: M. Deleuil.

twice the transit duration before its ingress and after its egress. For Kepler-39, a linear function of time did not provide a satisfactory normalisation because of the short-term stellar variability (see Sect. 4.2), hence a quadratic function of time was used. Correlated noise was estimated following Pont et al. (2006) and Bonomo et al. (2012b), and added in quadrature to the formal error bars. However, it turned out to be very low, generally lower than one fifth of the formal photometric errors, as expected for high-precision space-based photometry (e.g., Aigrain et al. 2009; Bonomo et al. 2012b).

Our global model has 12 free parameters when i) an eccentric model was considered and ii) RV were taken with only one instrument (SOPHIE): the transit epoch T_0; the orbital period P; the systemic radial velocity V_r; the radial-velocity semi-amplitude K; $\sqrt{e}\cos\omega$ and $\sqrt{e}\sin\omega$ (e.g., Anderson et al. 2011); an additive RV jitter term s_j to account for possible jitter in the RV measurements regardless of its origin, such as instrumental effects, stellar activity, additional companions, etc.; the transit duration from first to fourth contact T_{14}; the ratio of the planetary-to-stellar radii R_p/R_*; the inclination i between the orbital plane and the plane of the sky; and the two limb-darkening coefficients (LDC) $q_1 = (u_a + u_b)^2$ and $q_2 = 0.5u_a/(u_a + u_b)$ (Kipping 2013), where u_a and u_b are the coefficients of the limb-darkening quadratic law[5]. Two additional parameters, that is the HARPS-N systemic radial velocity and jitter term, were fitted when HARPS-N data were obtained as well (Kepler-74 and Kepler-75). Uniform priors were set on all parameters, in particular with bounds of [0, 1] for q_1 and q_2 (Kipping 2013), lower limit of zero for K and s_j, and upper bound of 1 for e (the lower limit of 0 simply comes from the choice of fitting $\sqrt{e}\cos\omega$ and $\sqrt{e}\sin\omega$).

The posterior distributions of our free parameters were determined by means of our DE-MCMC code by maximising a Gaussian likelihood (see, e.g., Eqs. (9) and (10) in Gregory 2005). For each target, a number of chains equal to twice the number of free parameters were run simultaneously after being started at different positions in the parameter space but reasonably close to the system values known in the literature and/or obtained with an independent fit that was previously performed with AMOEBA (Nelder & Mead 1965). The jumps for a current chain in the parameter space were determined from the other chains, according to the prescriptions given by Ter Braak (2006), and the Metropolis-Hastings algorithm was used to accept or reject a proposed step for each chain.

For the convergence of the chains, we required the Gelman-Rubin statistics, $\hat{R}$, to be lower than 1.03 for all the parameters (Gelman et al. 2003). Steps belonging to the burn-in phase were identified following Knutson et al. (2009) and were excluded. The medians of the posterior distributions of the fitted and derived parameters and their 34.13% intervals are reported as the final values and their 1σ error bars. When the distributions of the eccentricity and the RV jitter were found to peak at zero, we provided only the 1σ upper limits estimated as the 68.27% confidence intervals starting from zero. Indeed, the medians of these distributions might yield misleading non-zero values.

Finally, the Yonsei-Yale evolutionary tracks (Demarque et al. 2004) for the effective temperature, metallicity, and density of the host stars were used to determine the stellar, hence companion, parameters (Sozzetti et al. 2007; Torres et al. 2012).

[5] $I(\mu)/I(1) = 1 - u_a(1-\mu) - u_b(1-\mu)^2$, where $I(1)$ is the specific intensity at the centre of the disc and $\mu = \cos\gamma$, γ being the angle between the surface normal and the line of sight.

For Kepler-41 and Kepler-74 only a circular model was adopted for the following reasons: the RV curve of Kepler-41 is slightly asymmetric with respect to a sinusoid, very likely because of residual effects from the correction of moonlight contamination and/or low S/N (from 13 to 20) spectra. These artificial asymmetries in the RV curve tend to bias the solution of system parameters towards a low but non-zero eccentricity $e \sim 0.14$ even when including in the global fit the secondary eclipse that indicates that $e\cos\omega$ is consistent with zero (e.g., Santerne et al. 2011a; Quintana et al. 2013). This would reduce the orbital configurations of a possible eccentric orbit to $\omega = 90$ or 270 deg. However, the expected circularization timescale is shorter than 100 Myr by assuming a modified tidal quality factor of $Q'_p = 10^7$ for the planet because of its short orbital period $P = 1.85$ days (hence small semi-major axis $a = 0.031$ au) and relatively low mass $M_p \sim 0.6\ M_{Jup}$ for a Jupiter-sized planet. Indeed, there are no planets with mass comparable to Kepler-41 and $P < 3$ d with a significant eccentricity. For these reasons, we adopted a circular model for Kepler-41.

For Kepler-74, our DE-MCMC chains did not converge towards a unique solution when we varied the eccentricity, which resulted in very low acceptance rates. This was also noticed by Hébrard et al. (2013), who imposed a Gaussian prior on the orbital eccentricity, solely based on a RV fit, in their combined analysis of *Kepler* and RV data. However, this prior inevitably affects the posterior distributions of orbit and transit parameters. Instead, we preferred to use a circular model given that current RV data evidently do not allow us to constrain the orbital eccentricity well.

The Kepler-39 system parameters were obtained by using both eccentric and circular models because the 2σ significance of the eccentricity $e = 0.112 \pm 0.057$ cannot exclude that the orbit is perfectly circular (Lucy & Sweeney 1971).

4. Results

4.1. Stellar atmospheric parameters

The T_{eff} and [Fe/H] of Kepler-41, Kepler-43, Kepler-44, and Kepler-74, which were determined with the procedure described in Sect. 3.1, are consistent within 1σ with the literature values. The surface gravities of Kepler-43 and Kepler-44 were found to be $\log g = 4.4 \pm 0.10$ (Kepler-43) and $\log g = 4.1 \pm 0.10$ (Kepler-44), which are lower than previously found by Bonomo et al. (2012a), that is $\log g = 4.64 \pm 0.103$ and 4.59 ± 0.14, respectively. These newly determined values are more consistent with the photometrically derived $\log g$ (see Tables 4 and 5).

The star KOI-205 was found to be slightly hotter than reported by Díaz et al. (2013), with $T_{eff} = 5400 \pm 75$ K, metallicity [Fe/H] $= 0.18 \pm 0.12$, and $\log g = 4.7 \pm 0.10$, both with the ESPaDOnS and the co-added SOPHIE spectrum (see Table 8). The slightly hotter temperature has only a minor, almost negligible, influence on system parameters.

The most striking differences with previously determined atmospheric parameters were found for Kepler-39 and Kepler-75. The former is significantly richer in metals and slightly hotter than reported by Bouchy et al. (2011): $T_{eff} = 6350 \pm 100$ K, [Fe/H] $= 0.10 \pm 0.14$, and $\log g = 4.4 \pm 0.15$, to be compared with the previous estimates $T_{eff} = 6260 \pm 140$, [Fe/H] $= -0.29 \pm 0.10$, and $\log g = 4.1 \pm 0.2$. Very consistent values were derived from the analysis of the ESPaDOnS spectrum. This difference comes from the better selection and treatment of the SOPHIE spectra before co-adding the individual spectra (see Sect. 2.3). It is not due to the different spectral analysis technique that was used by

Bouchy et al. (2011), that is, the VWA package (Bruntt et al. 2010). Indeed, when run on the new co-added SOPHIE spectrum, VWA provided results that are almost identical to those obtained with MOOG: $T_{\rm eff}$ = 6360 ± 100 K, [Fe/H] = 0.12 ± 0.14, and $\log g$ = 4.4 ± 0.3. These new values have an impact on stellar mass and age (see Table 2).

Kepler-75 is also found to be richer in metals than previously thought. Its atmospheric parameters determined with MOOG are $T_{\rm eff}$ = 5200±100 K, [Fe/H] = 0.30±0.12, and $\log g$ = 4.6±0.15. While the $T_{\rm eff}$ is consistent within 1σ with the value derived by Hébrard et al. (2013), the difference in metallicity is about 2σ (see Table 7). However, at these temperatures, the system parameters of Kepler-75 do not significantly change as a consequence of the higher metallicity.

4.2. System parameters

4.2.1. Kepler-39

Orbital and transit parameters obtained with our Bayesian DE-MCMC analysis in the eccentric case agree well with those that were previously determined by Bouchy et al. (2011). However, we found a lower significance of approximately 2σ for the orbital eccentricity, that is e = 0.112 ± 0.057, while Bouchy et al. (2011) reported e = 0.122 ± 0.023. Our larger uncertainty on the eccentricity indicates that it might be spurious, according to Lucy & Sweeney (1971). The Bayes factor of ∼3 between the eccentric and the circular model, which was computed by using the truncated posterior mixture method (Tuomi & Jones 2012), does not provide strong enough evidence either for an eccentric orbit, according to Kass & Raftery (1995).

As discussed in Sect. 4.1, the stellar atmospheric parameters were refined thanks to both a better treatment of the SOPHIE spectra and a new ESPaDOnS spectrum. Specifically, a moderately hotter temperature $T_{\rm eff}$ = 6350 ± 100 K and a significantly higher metallicity of 0.10 ± 0.14 were found (see Sect. 4.1). For these new atmospheric parameters and the transit density, the Yonsei-Yale evolutionary tracks indicate a more massive and younger star: $M_\star = 1.29^{+0.06}_{-0.07}$ $M_\odot$, $R_\star$ = 1.40 ± 0.10 $R_\odot$, and age of $2.1^{+0.8}_{-0.9}$ Gyr. The corresponding mass, radius, and density of Kepler-39b are $M_{\rm b} = 20.1^{+1.3}_{-1.2}$ $M_{\rm Jup}$, $R_{\rm b} = 1.24^{+0.09}_{-0.10}$ $R_{\rm Jup}$, and $\rho_{\rm b} = 13.0^{+3.0}_{-2.2}$ g cm^{-3}. These companion parameters are consistent with those reported by Bouchy et al. (2011), except for the stellar age, which is about half the value found by these authors (see Table 2). Interestingly, this updated value of the age agrees well with the gyrochronology estimate (Mamajek & Hillenbrand 2008), that is $t_{\rm gyr} = 0.7^{+0.9}_{-0.3}$ Gyr, for the stellar rotation period $P_{\rm rot}$ = 4.50 ± 0.07 d inferred from the *Kepler* LC light curve.

Figure 1 shows the position of Kepler-39b (empty red circle) in the radius-mass diagram of transiting companions with masses between 10 and 100 $M_{\rm Jup}$ for the eccentric case. The dashed lines from top to bottom show the Baraffe et al. (2003) isochrones for 0.5, 1, 5, and 10 Gyr. As already noted by Bouchy et al. (2011), the companion radius given by the eccentric solution would be incompatible with theoretical isochrones with a probability >95% (2σ). However, the solution these authors proposed to explain the large radius of Kepler-39b, that is an increased opacity in the companion atmosphere, which previously seemed unlikely for the low stellar metallicity, now might apply for Kepler-39b. Indeed, our new estimate of [Fe/H] is significantly higher.

As previously discussed, the eccentricity of Kepler-39b might be spurious. In the circular case, stellar and companion radii are slightly smaller than in the eccentric case, which implies a higher bulk density of $17.4^{+1.6}_{-1.4}$ g cm^{-3} (see Table 2). The system age would be $1.0^{+0.9}_{-0.7}$ Gyr. The position of Kepler-39b in the circular case is shown in Fig. 1 with a red filled circle. Figure 2 displays the phase-folded transit and RV curve and the best solutions obtained with both eccentric and circular models.

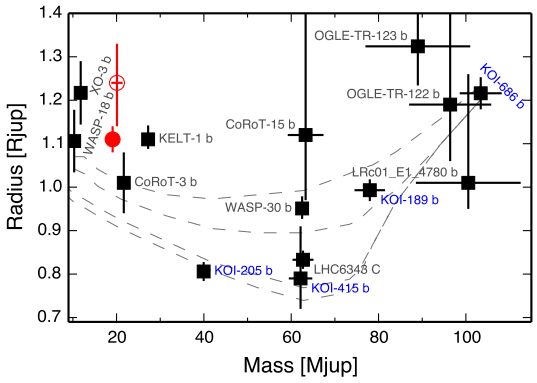

Fig. 1. Radius-mass diagram including transiting companions more massive than 10 $M_{\rm Jup}$. The dashed curves are the Baraffe et al. (2003) isochrones for 0.5, 1, 5, and 10 Gyr (from top to bottom). Both circular (filled red circle) and eccentric (empty red circle) solutions are shown for Kepler-39b. Blue labels indicate the brown dwarfs and low-mass stars that were characterized thanks to SOPHIE spectroscopic measurements (see also Moutou et al. 2013; Díaz et al. 2014).

4.2.2. Kepler-41

The new system parameters determined with SC data significantly differ from those obtained by Santerne et al. (2011a). The most important difference in the fitted parameters is found for the orbital inclination that, in turn, affects the determination of $a/R_\star$ and the stellar density. Indeed, while Santerne et al. (2011a) found i = 88.3 ± 0.7 deg, our new solution points to a considerably higher impact parameter with i = 82.51 ± 0.09 deg (see Table 3).

By analysing only LC data, Southworth (2012) found two solutions for the orbital inclination, one with $i \sim 90$ deg and the other one with $i \sim 80$–82 deg. He opted for the first because "the $i \sim 80$–82 deg family occurs mainly for LD-fixed light-curve solutions, and results in weird physical properties". However, by letting the LDC vary in the SC transit fitting, the DE-MCMC chains always converged toward the latter value of i. This occurred even when the chains were all started at values close to $i \sim 90$ deg. This ambivalence shows that, in some cases, fitting the LDC with LC data may lead to local minima that do not represent the true solution.

Long-cadence measurements were also used by Quintana et al. (2013) to validate this planet by analysing the phase curve. Curiously, these authors found an orbital inclination of $85.4^{+0.4}_{-0.5}$ deg, which is in between the other two solutions. However, we point out that Quintana et al. (2013) were more interested in analysing the phase curve and did not explicitly mention which oversampling they adopted to model the LC transits.

Our solution with low orbital inclination i = 82.5 deg is physically acceptable because the lowest possible inclination for the transit of Kepler-41b is ∼78 deg. The corresponding stellar density indicates a star that is larger and older than previously found for the same atmospheric parameters. The derived $\log g$ = 4.278 ± 0.005 is now more consistent with the spectroscopic value $\log g$ = 4.2 ± 0.10 (see Table 3). A larger stellar radius

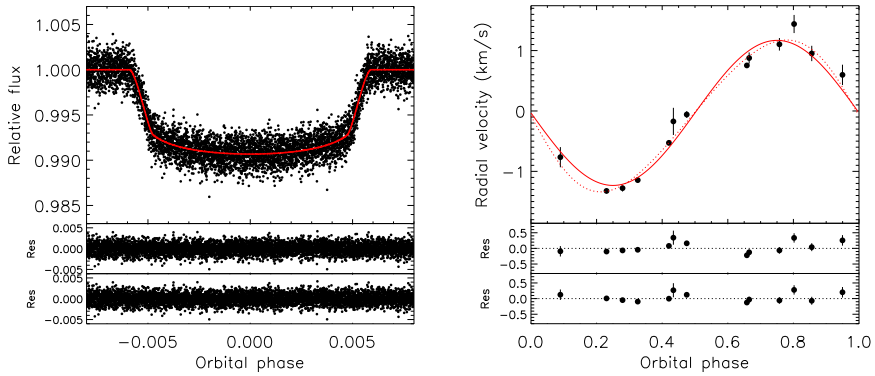

Fig. 2. *Left panel. Top*: phase-folded transit of Kepler-39b along with the transit models for the circular (red solid line) and eccentric (red dotted line) orbits. The two models are indistinguishable. *Middle*: residuals of the circular orbit. *Bottom*: residuals of the eccentric orbit. *Right panel. Top*: phase-folded radial-velocity curve of Kepler-39 and, superimposed, the Keplerian models for the circular (red solid line) and eccentric (red dotted line) orbits. *Middle*: O–C of the circular orbit. *Bottom*: O–C of the eccentric orbit.

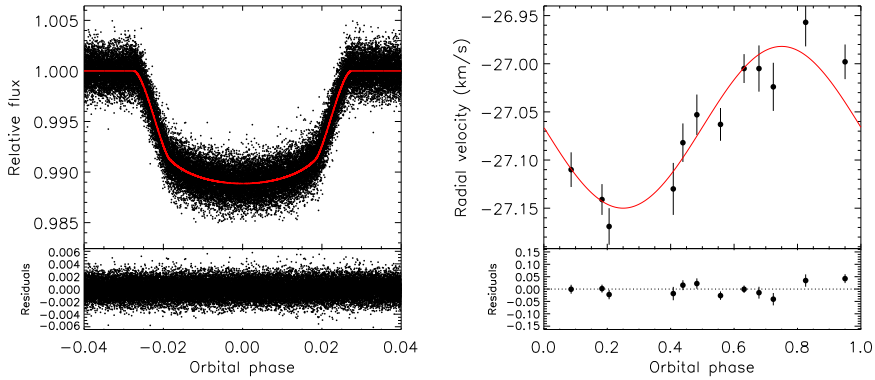

Fig. 3. *Left panel*: phase-folded transit light curve of Kepler-41b along with the transit model (red solid line). *Right panel*: phase-folded radial-velocity curve of Kepler-41 and, superimposed, the Keplerian model (red solid line).

implies a larger planetary radius $R_p = 1.29 \pm 0.02\ R_{Jup}$, which now makes this planet more similar to the other close-in hot Jupiters. Indeed, from the planetary parameters that were previously determined by Santerne et al. (2011a) and Southworth (2012), this object appeared quite rare, meaning: non-inflated despite its vicinity to the parent star (see Figs. 9 and 10 in Santerne et al. 2011a).

Figure 3 displays the phase-folded transit and RV measurements along with the best solution.

Last but not least, the lower inclination also has an impact on a/R_p that becomes equal to 50.26 ± 0.36 and, in turn, affects the determination of the geometric albedo (cf., e.g., Eq. (14) in Rowe et al. 2006). The latter was found to be considerably higher than the majority of hot Jupiters with measured optical occultations by Santerne et al. (2011a), that is $A_g = 0.30 \pm 0.07$. On the contrary, our new solution with SC data indicates a significantly lower geometric albedo of $A_g < 0.135$ from the most recent value of the secondary-eclipse depth (Angerhausen et al. 2014), in agreement with theoretical expectations for atmospheres of hot Jupiters without scattering clouds (e.g., Burrows et al. 2008). Figure 4 shows the albedo values and their 1σ uncertainties as a function of the planet day-side equilibrium temperature T_{eq}. The vertical dashed lines indicate the values of T_{eq} assuming perfect heat redistribution (left) or no redistribution in the atmosphere (right).

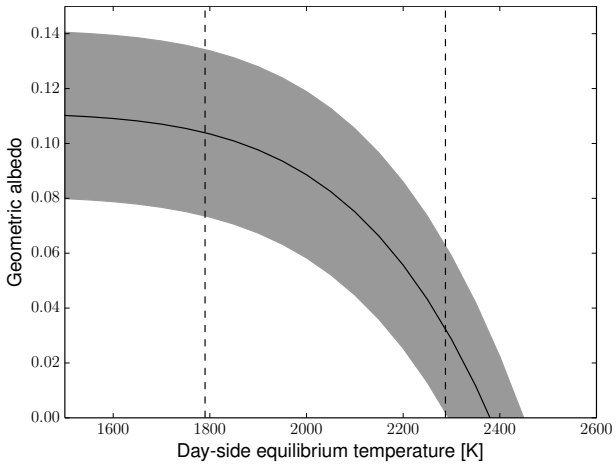

Fig. 4. Geometric albedo of Kepler-41b as a function of its day-side equilibrium temperature. T_{eq}. The vertical dashed lines indicate the values of T_{eq} assuming perfect heat redistribution (*left*) and no redistribution in the atmosphere (*right*). The grey band shows the albedo values allowed by the 1σ uncertainty on the occultation depth determined by Santerne et al. (2011a).

4.2.3. Kepler-43

System parameters derived from our DE-MCMC analysis are listed in Table 4, and Fig. 5 shows the phase-folded SC transit and RV curve along with the best-fit model. System parameters generally agree within 1σ with those determined by Bonomo et al. (2012a), in spite of the very poor sampling of the phase-folded LC transit (see their Fig. 5). The transit duration derived with SC data is slightly shorter (at 1.3σ) than found by Bonomo et al. (2012a) but with negligible influence on system parameters. The planet eccentricity is consistent with zero within 2σ.

From the stellar rotation period $P_{rot} = 12.95 \pm 0.25$ d derived with all the LC data, the gyrochronology age $t_{gyr} = 1.7^{+0.6}_{-0.4}$ Gyr agrees well with that estimated from stellar evolutionary tracks $2.3^{+0.8}_{-0.7}$ Gyr, as already noted by Bonomo et al. (2012a).

4.2.4. Kepler-44

New system parameters slightly differ from those derived by Bonomo et al. (2012a) (see Table 5). Our analysis with SC data

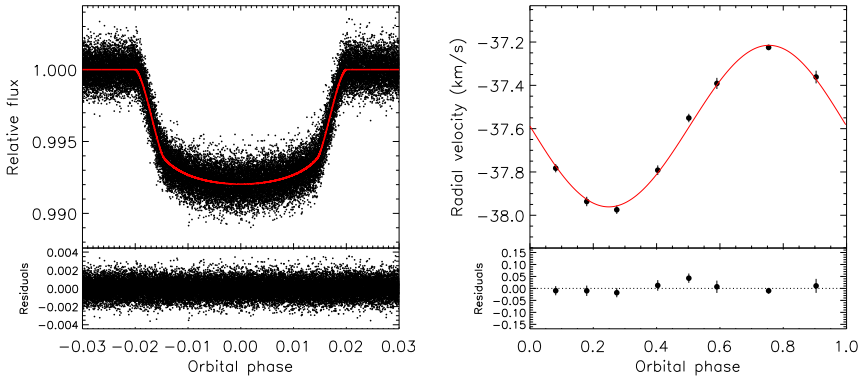

Fig. 5. *Left panel*: phase-folded transit light curve of Kepler-43b along with the transit model (red solid line). *Right panel*: phase-folded radial-velocity curve of Kepler-43 and, superimposed, the Keplerian model (red solid line).

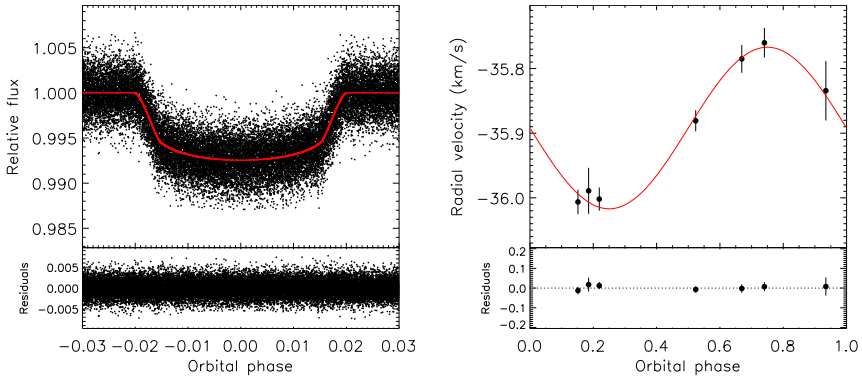

Fig. 6. *Left panel*: phase-folded transit light curve of Kepler-44b along with the transit model (red solid line). *Right panel*: phase-folded radial-velocity curve of Kepler-44 and, superimposed, the Keplerian model (red solid line).

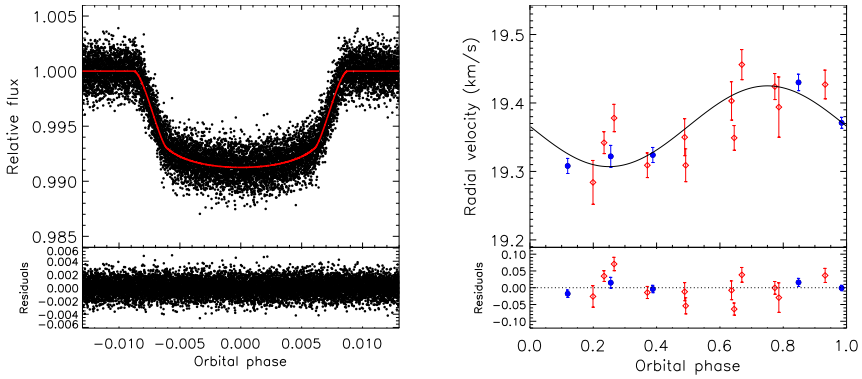

Fig. 7. *Left panel*: phase-folded transit light curve of Kepler-74b along with the transit model for a circular orbit and their residuals. *Right panel*: phase-folded radial-velocity curve of Kepler-74. Red diamonds and blue circles show SOPHIE and HARPS-N radial velocities, respectively. The black solid line displays the Keplerian circular model.

reveals a transit duration that is 2σ shorter than found by Bonomo et al. (2012a). This implies a slightly larger $a/R_\star$, hence a moderately higher stellar density from the Kepler's third law. In consequence, stellar evolutionary tracks point to a slightly smaller star than previously reported by Bonomo et al. (2012a), with radius and mass of 1.35 ± 0.08 $R_\odot$ and 1.12 ± 0.08 $M_\odot$, respectively. Therefore, also the planet turns out to be smaller (from $R_p/R_\star$) and denser: $R_p = 1.09 \pm 0.07$ R_{Jup}, $M_p = 1.00 \pm 0.10$ M_{Jup}, and $\rho_p = 0.93^{+0.19}_{-0.17}$ g cm^{-3} (see Table 5).

Figure 6 shows the phase-folded transit and RV curve and, superimposed, the transit and the Keplerian models.

4.2.5. Kepler-74

The circular solution we decided to adopt differs from the eccentric system parameters by almost three standard deviations. This is mainly because the transit density used to determine stellar parameters is a function of the eccentricity. For a null eccentricity, the planet becomes smaller and denser, with $R_p = 0.97 \pm 0.04$ R_{Jup}, $M_p = 0.64 \pm 0.10$ M_{Jup}, and $\rho_p = 0.86 \pm 0.18$ g cm^{-3}. The best fit of the transit and radial velocities is displayed in Fig. 7.

4.2.6. Kepler-75

The agreement between the system parameters determined by Hébrard et al. (2013) and our DE-MCMC solution obtained with SC data (see Table 7) is excellent, even adopting the slightly different atmospheric parameters derived with MOOG: $T_{eff} = 5200 \pm 100$ K and [Fe/H] $= 0.30 \pm 0.12$.

The stellar rotation period inferred from the whole LC light curve is $P_{rot} = 19.18 \pm 0.15$ d, in agreement with Hébrard et al. (2013). The system age estimated from gyrochronology (Mamajek & Hillenbrand 2008) is 1.6±0.3 Gyr, which is slightly lower than the value provided by stellar models, although consistent with the latter at 1.7σ.

The transit and RV data along with the best solutions are shown in Fig. 8.

4.2.7. KOI-205

As for Kepler-75, the SC orbital and physical parameters agree very well with those determined by Díaz et al. (2013) (see Table 8). The best fit of the SC transit and RV observations is shown in Fig. 9.

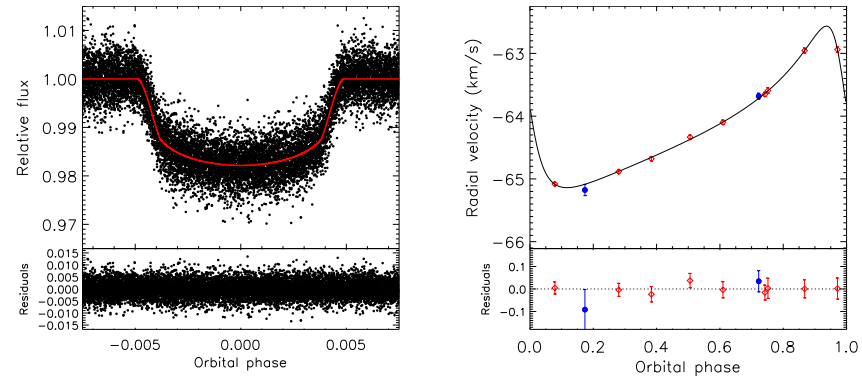

Fig. 8. *Left panel*: phase-folded transit light curve of Kepler-75b along with the transit model (red solid line). *Right panel*: phase-folded radial-velocity curve of Kepler-75. Red diamonds and blue circles show SOPHIE and HARPS-N radial velocities, respectively. The black solid line displays the Keplerian model.

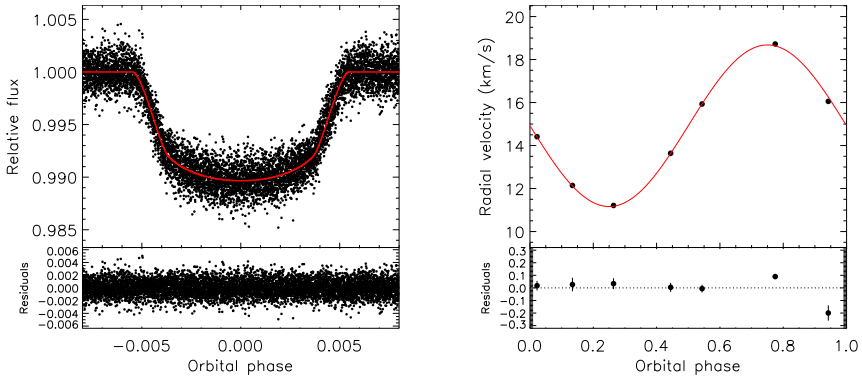

Fig. 9. *Left panel*: phase-folded transit light curve of KOI-205 along with the transit model (red solid line). *Right panel*: phase-folded radial-velocity curve of KOI-205 and, superimposed, the Keplerian model (red solid line).

5. Discussion and conclusions

The analysis of *Kepler* SC photometry, RV data, SOPHIE and ESPaDONs spectra of seven giant companions has permitted us to refine their orbital and physical parameters. In three cases, namely Kepler-43, Kepler-75, and KOI-205, they agree with published parameters within $1-1.3\sigma$.

For Kepler-44, for which only two quarters of LC data (Q1 and Q2) were analysed for the discovery announcement, the new transit parameters determined with our DE-MCMC approach indicate a transit duration shorter by 2σ, hence a slightly larger $a/R_\star$ and higher stellar density. This, in turn, implies that the host star and its planetary companion are smaller than previously found.

A separate discussion must be made for Kepler-39b and Kepler-74b because we have revised the significance of their orbital eccentricities. That of Kepler-39b is detected with a 2σ significance level and, according to the Lucy-Sweeney criterion, it might be spurious. Slight asymmetries in the RV curve caused by residual effects from the correction of moonlight contamination (Santerne et al. 2011b) and/or CCD charge transfer inefficiency (Bouchy et al. 2009) might cause false eccentricities. Indeed, these effects become strong when observing faint stars. More RV observations without moonlight contamination are required to determine whether Kepler-39b has a low eccentricity. Kepler-74 would also benefit from additional high-accuracy and high-precision RVs because the chains of our DE-MCMC combined analysis did not converge towards a unique solution when including the eccentricity as a free parameter. For this reason, we decided to fit only a circular model to *Kepler* and RV data. For circular orbits, both Kepler-39b and Kepler-74b would be smaller and denser than previously found. In any case, the radius of Kepler-39b is still larger than predicted by theoretical isochrones (see Fig. 1), as highlighted by Bouchy et al. (2011).

Our new spectral analyses of the available co-added spectra revealed slightly hotter effective temperatures of Kepler-39 and KOI-205 and significantly higher metallicities for Kepler-39 and Kepler-75.

Among our seven targets, the most striking divergence with already published parameters was found for Kepler-41. Indeed, SC data point to a considerably lower inclination, higher impact parameter, and lower $a/R_\star$ than found by Santerne et al. (2011a) and Southworth (2012). In consequence, both the host star and the planet have larger radii than previously derived. This new solution also has an impact on the estimation of the planetary geometric albedo that is significantly lower than previously estimated: $A_g < 0.135$. Both the larger radius and the lower albedo make this planet resemble the majority of hot Jupiters. Conversely, the analysis of *Kepler* LC data had erroneously resulted in peculiar characteristics for this planet. This emphasizes that, in some cases, SC data are necessary to derive accurate system parameters, in addition to reducing covariances between transit parameters (Price & Rogers 2014) and permitting to compute precise transit timing variations. This will also be considered in the light of the future TESS and PLATO space missions.

Acknowledgements. A. S. Bonomo and R. F. Díaz acknowledge funding from the European Union Seventh Framework Programme (FP7/2007–2013) under Grant agreement number 313014 (ETAEARTH). A. Santerne is supported by the European Union under a Marie Curie Intra-European Fellowship for Career Development with reference FP7-PEOPLE-2013-IEF, number 627202. This research has made use of the results produced by the PI2S2 Project managed by the Consorzio COMETA, a co-funded project by the Italian Ministero dell'Istruzione, Università e Ricerca (MIUR) within the Piano Operativo Nazionale Ricerca Scientifica, Sviluppo Tecnologico, Alta Formazione (PON 2000Ð2006).

References

Aigrain, S., Pont, F., Fressin, F., et al. 2009, A&A, 506, 425
Anderson, D. R., Collier Cameron, A., Hellier, C., et al. 2011, ApJ, 726, L19

Angerhausen, D., DeLarme, E., Morse, J. A., et al. 2014, ApJ, submitted [arXiv:1404.4348]
Baraffe, I., Chabrier, G., Barman, T. S., et al. 2003, A&A, 402, 701
Burke, C. J., Bryson, S. T., Mullally, F., et al. 2014, ApJS, 210, 19
Bonomo, A. S., Santerne, A., Alonso, R., et al. 2010, A&A, 520, A65
Bonomo, A., S., Hébrard, G., Santerne, A., et al. 2012a, A&A, 538, A96
Bonomo, A., S., Chabaud, P.-Y., Deleuil, M., et al. 2012b, A&A, 547, A110
Bouchy, F., Hébrard, G., Udry, S., et al. 2009, A&A, 505, 853
Bouchy, F., Bonomo, A. S., Santerne, A., et al. 2011, A&A, 533, A83
Bruntt, H., Bedding, T. R., Quirion, P.-O., et al. 2010, MNRAS, 405, 1907
Burrows, A., Ibgui, L., & Hubeny, I. 2008, ApJ, 682, 1277
Cosentino, R., Lovis, C., Pepe, F., et al. 2012, in SPIE Conf. Ser., 8446
Demarque, P., Woo, J.-H., Kim, Y.-Ch. & Yi S. K. 2004, ApJS, 155, 667
Díaz, R. F., Damiani, C., Deleuil, M., et al. 2013, A&A, 551, L9
Díaz, R. F., Montagnier, G., Leconte, J., et al. 2014, A&A, 572, A109
Eastman, J., Siverd, R., & Gaudi, B. S. 2010, PASP, 122, 935
Eastman, J., Gaudi, B. S., & Agol, E. 2013, PASP, 125, 923
Gelman A., Carlin J. B., Stern H. S., & Rubin D. B. 2004, Bayesian data analysis, 2nd edn. (London: Chapman & Hall)
Giménez, A. 2006, A&A, 450, 1231
Giménez, A. 2009, in The Eighth Pacific Rim Conference on Stellar Astrophysics: A Tribute to Kam Ching Leung, eds. B. Soonthornthum, S. Komonjinda, K. S. Cheng, & K. C. Leung (San Francisco: ASP), 450, 291
Gonzalez, G., & Vanture, A. D. 1998, A&A, 339, L29
Gregory, P. C. 2005, ApJ, 631, 1198
Hébrard, G., Almenara, J.-M., Santerne, A., et al. 2013, A&A, 554, A114
Jenkins, J. M., Caldwell, D. A., Chandrasekaran, H., et al. 2010, ApJ, 713, L87
Jordán, A., & Bakos, G. Á. 2008, ApJ, 685, 543
Kang, W., & Lee, S.-G. 2012, MNRAS, 425, 3162
Kass, R. E., & Raftery, A. E. 1995, J. Am. Stat. Ass., 430, 773
Kipping, D. 2010, MNRAS, 408, 1758
Kipping, D. 2013, MNRAS, 435, 2152
Kipping, D., & Bakos, G. 2011, ApJ, 730, 50
Knutson, H. A., Charbonneau, D., Cowan, N. B., et al. 2009, ApJ, 703, 769
Kurucz, R. I. 1993, ATLAS9 Stellar Atmosphere Programs and 2 km s^{-1} grid, Kurucz CD-ROM No. 13 (Cambridge, Mass.: Smithsonian Astrophysical Observatory)
Lucy, L. B., & Sweeney, M. A., et al. 1971, AJ, 76, 544
Mamajek, E. E., & Hillenbrand, L. 2008, ApJ, 687, 1264
Mortier, A., Santos, N. C., Sousa, S. G., et al. 2013, A&A, 558, A106
Moutou, C., Bonomo, A. S., Bruno, G., et al. 2013, A&A, 558, L6
Nelder, J. A., & Mead, R. 1965, Comput. J., 7, 308
Neuforge-Verheecke, C., & Magain, P. 1997, A&A, 328, 261
Pont, F., Zucker, S., & Queloz, D. 2006, MNRAS, 373, 231
Price, E. M., & Rogers, L. A. 2014, ApJ, 794, 92
Quintana, E., Rowe, J. F., Barclay, T., et al. 2013, ApJ, 767, 137
Rowe, J. F., Matthews, J. M., Seager, S., et al. 2006, ApJ, 646, 1241
Santerne, A., Bonomo, A. S., Hébrard, G., et al. 2011a, A&A, 536, A70
Santerne, A., Endl, M., Hatzes, A., et al. 2011b, Detection and Dynamics of Transiting Planets, Proc. Haute-Provence Observatory Colloquium, eds. F. Bouchy, R. F. Díaz, & C. Moutou, EPJ Web Conf., 11, 02001
Santerne, A., Díaz, R. F., Moutou, C., et al. 2012, A&A, 545, A76
Sekiguchi, M., & Fukugita, M. 2000, ApJ, 120, 1072
Sing, D. K. 2010, A&A, 510, A21
Sneden, C. A. 1973, Ph.D. Thesis, The University of Texas at Austin
Sozzetti, A., Yong, D., Torres, G., et al. 2004, ApJ, 616, L167
Sozzetti, A., Yong, D., Carney, B. W., et al. 2006, AJ, 131, 2274
Sozzetti, A., Torres, G., Charbonneau, D., et al. 2007, ApJ, 664, 1190
Southworth, J. 2011, MNRAS, 417, 2166
Southworth, J. 2012, MNRAS, 426, 1292
Ter Braak, C. J. F. 2006, Stat. Comput., 16, 239
Torres, G., Fischer, D. A., Sozzetti, A., et al. 2012, ApJ, 757, 161
Tuomi, M., & Jones, H. R. A. 2012, A&A, 544, A116
Winn, J. 2010, in Exoplanets, ed. S. Seager (Tucson, AZ: University of Arizona Press) [arXiv:1001.2010]
Zechmeister, M., & Kürster, M. 2009, A&A, 496, 577

Pages 10 to 16 are available in the electronic edition of the journal at http://www.aanda.org

Table 2. Kepler-39 system parameters.

Fitted system parameters	Bouchy et al. (2011)	This work (eccentric)	This work (circular)
Orbital period P [days]	21.0874 ± 0.0002	21.087210 ± 0.000037	21.087212 ± 0.000030
Transit epoch T_0[BJD$_{\rm TDB}$ − 2 454 900]	72.5959 ± 0.0006	1042.60708 ± 0.00024	1042.60707 ± 0.00021
Transit duration T_{14} [h]	6.02 ± 0.09	5.960 ± 0.020	5.960 ± 0.016
Radius ratio $R_{\rm b}/R_*$	$0.0896^{+0.0011}_{-0.0012}$	$0.0910^{+0.0006}_{-0.0008}$	0.0911 ± 0.0006
Inclination i [deg]	$88.83^{+0.59}_{-0.40}$	89.07 ± 0.22	$89.23^{+0.13}_{-0.11}$
Limb-darkening coefficient q_1	–	$0.23^{+0.08}_{-0.06}$	$0.22^{+0.06}_{-0.05}$
Limb-darkening coefficient q_2	–	$0.32^{+0.14}_{-0.10}$	$0.33^{+0.12}_{-0.09}$
$\sqrt{e}\ \cos\omega$	–	$-0.047^{+0.084}_{-0.078}$	0 (fixed)
$\sqrt{e}\ \sin\omega$	–	$0.324^{+0.080}_{-0.132}$	0 (fixed)
Orbital eccentricity e	0.122 ± 0.023	0.112 ± 0.057	0 (fixed)
Argument of periastron [deg] ω	$98.9^{+5.9}_{-6.8}$	99^{+22}_{-14}	90 (fixed)
Radial-velocity semi-amplitude K [km s^{-1}]	1.251 ± 0.030	1.257 ± 0.064	1.201 ± 0.050
Systemic velocity $V_{\rm r}$ [km s^{-1}]	$-0.101^{+0.017}_{-0.015}$	−0.063 ± 0.044	$-0.032^{+0.040}_{-0.037}$
RV jitter [m s^{-1}] $s_{\rm j}$	–	108^{+56}_{-40}	140^{+40}_{-33}
Derived transit parameters			
a/R_*	$23.8^{+1.8}_{-1.7}$	$24.92^{+1.9}_{-1.5}$	$27.74^{+0.55}_{-0.49}$
Stellar density ρ_* [g cm^{-3}]	$0.57^{+0.14}_{-0.11}$	$0.66^{+0.15}_{-0.11}$	$0.91^{+0.06}_{-0.05}$
Impact parameter b	$0.43^{+0.11}_{-0.18}$	$0.36^{+0.05}_{-0.08}$	$0.37^{+0.04}_{-0.06}$
Limb-darkening coefficient u_a	0.303 ± 0.014[a]	0.31 ± 0.07	0.32 ± 0.06
Limb-darkening coefficient u_b	0.308 ± 0.005[a]	0.17 ± 0.14	0.15 ± 0.11
Atmospheric parameters of the star			
Effective temperature $T_{\rm eff}$[K]	6260 ± 140	6350 ± 100	6350 ± 100
Spectroscopic surface gravity log g [cgs]	4.1 ± 0.2	4.40 ± 0.15	4.40 ± 0.15
Derived surface gravity log g [cgs]	4.19 ± 0.07	4.25 ± 0.06	4.34 ± 0.02
Metallicity [Fe/H] [dex]	–0.29 ± 0.10	0.10 ± 0.14	0.10 ± 0.14
Stellar rotational velocity $V \sin i_*$ [km s^{-1}]	16 ± 2.5	16 ± 2.5	16 ± 2.5
Spectral type	F8IV	F7V	F7V
Stellar and planetary physical parameters			
Stellar mass [$M_\odot$]	$1.10^{+0.07}_{-0.06}$	$1.29^{+0.06}_{-0.07}$	$1.26^{+0.07}_{-0.06}$
Stellar radius [$R_\odot$]	1.39 ± 0.11	1.40 ± 0.10	1.25 ± 0.03
Companion mass $M_{\rm b}$ [$M_{\rm Jup}$]	18.0 ± 0.9	$20.1^{+1.3}_{-1.2}$	19.1 ± 1.0
Companion radius $R_{\rm b}$ [$R_{\rm Jup}$]	$1.22^{+0.12}_{-0.10}$	$1.24^{+0.09}_{-0.10}$	1.11 ± 0.03
Companion density $\rho_{\rm b}$ [g cm^{-3}]	$12.4^{+3.4}_{-2.6}$	$13.0^{+3.0}_{-2.2}$	$17.4^{+1.6}_{-1.4}$
Companion surface gravity log $g_{\rm b}$ [cgs]	4.48 ± 0.09	4.51 ± 0.05	4.58 ± 0.03
Age t [Gyr]	5.1 ± 1.5	$2.1^{+0.8}_{-0.9}$	$1.0^{+0.9}_{-0.7}$
Orbital semi-major axis a [au]	0.155 ± 0.003	0.164 ± 0.003	0.162 ± 0.003
Equilibrium temperature $T_{\rm eq}$ [K][b]	905 ± 39	897 ± 29	853 ± 14

Notes. [(a)] The limb-darkening coefficients were allowed to vary within their 1σ errors related to the uncertainties on stellar atmospheric parameters. [(b)] Black-body equilibrium temperature assuming a null Bond albedo and uniform heat redistribution to the night side.

Table 3. Kepler-41 system parameters.

Fitted system parameters	Santerne et al. (2011a)	This work
Orbital period P [days]	1.855558 ± 0.000007	$1.85555820 \pm 0.00000052$
Transit epoch T_0[BJD$_{\rm TDB}$ − 2 454 900]	70.1803 ± 0.0003	287.280482 ± 0.000051
Transit duration T_{14} [h]	2.376 ± 0.048	2.4341 ± 0.0046
Radius ratio $R_{\rm p}/R_*$	0.0895 ± 0.0019	0.10265 ± 0.00042
Inclination i [deg]	88.3 ± 0.7	82.51 ± 0.09
Limb-darkening coefficient q_1	–	0.39 ± 0.04
Limb-darkening coefficient q_2	–	$0.37^{+0.08}_{-0.07}$
Orbital eccentricity e	0 (fixed)	0 (fixed)
Radial-velocity semi-amplitude K [m s^{-1}]	85 ± 11	84 ± 11
Systemic velocity $V_{\rm r}$ [km s^{-1}]	-27.066 ± 0.007	-27.066 ± 0.008
RV jitter [m s^{-1}] $s_{\rm j}$	–	16^{+10}_{-9}
Derived transit parameters		
a/R_*	6.43 ± 0.05	5.159 ± 0.023
Stellar density ρ_* [g cm^{-3}]	1.46 ± 0.04	0.754 ± 0.010
Impact parameter b	0.19 ± 0.07	0.672 ± 0.005
Limb-darkening coefficient u_a	0.57 ± 0.13	0.46 ± 0.07
Limb-darkening coefficient u_b	0.41 ± 0.13	0.16 ± 0.10
Atmospheric parameters of the star		
Effective temperature $T_{\rm eff}$[K]	5620 ± 140	5750 ± 100
Spectroscopic surface gravity $\log g$ [cgs]	4.20 ± 0.15	4.20 ± 0.10
Derived surface gravity $\log g$ [cgs]	4.47 ± 0.12	4.278 ± 0.005
Metallicity [Fe/H] [dex]	0.29 ± 0.16	0.38 ± 0.11
Stellar rotational velocity $V \sin i_*$ [km s^{-1}]	6 ± 2	6 ± 2
Spectral type	G6V	G2V
Stellar and planetary physical parameters		
Stellar mass [$M_\odot$]	1.12 ± 0.07	1.15 ± 0.04
Stellar radius [$R_\odot$]	1.02 ± 0.03	1.29 ± 0.02
Planetary mass $M_{\rm p}$ [$M_{\rm Jup}$]	0.55 ± 0.09	0.56 ± 0.08
Planetary radius $R_{\rm p}$ [$R_{\rm Jup}$]	0.89 ± 0.05	1.29 ± 0.02
Planetary density $\rho_{\rm p}$ [g cm^{-3}]	1.10 ± 0.18	0.33 ± 0.04
Planetary surface gravity $\log g_{\rm p}$ [cgs]	3.23 ± 0.09	2.92 ± 0.06
Age t [Gyr]	$0.6^{+2.5}_{-0.3}$	$4.4^{+1.3}_{-1.1}$
Orbital semi-major axis a [au]	0.030 ± 0.010	0.03101 ± 0.0004
Equilibrium temperature $T_{\rm eq}$ [K][a]	1730 ± 40	1790 ± 31

Notes. [(a)] Black-body equilibrium temperature assuming a null Bond albedo and uniform heat redistribution to the night side.

Table 4. Kepler-43 system parameters.

Fitted system parameters	Bonomo et al. (2012a)	This work
Orbital period P [days]	3.024095 ± 0.000021	$3.02409309 \pm 0.00000020$
Transit epoch T_0[BJD$_{\rm TDB}$ − 2 454 900]	165.4159 ± 0.0006	195.45227 ± 0.00005
Transit duration T_{14} [h]	2.926 ± 0.019	2.900 ± 0.003
Radius ratio $R_{\rm p}/R_*$	$0.0868^{+0.0006}_{-0.0007}$	0.08647 ± 0.00019
Inclination i [deg]	$84.35^{+0.47}_{-0.40}$	$84.57^{+0.18}_{-0.37}$
Limb-darkening coefficient q_1	–	0.36 ± 0.02
Limb-darkening coefficient q_2	–	0.30 ± 0.04
$\sqrt{e}\,\cos\omega$	–	0.061 ± 0.030
$\sqrt{e}\,\sin\omega$	–	$0.086^{+0.12}_{-0.14}$
Orbital eccentricity e	<0.025	$0.017^{+0.027}_{-0.009}$
Argument of periastron [deg] ω	–	52^{+27}_{-81}
Radial-velocity semi-amplitude K [m s^{-1}]	375 ± 13	373 ± 9
Systemic velocity $V_{\rm r}$ [km s^{-1}]	-37.591 ± 0.007	-37.591 ± 0.007
RV jitter [m s^{-1}] $s_{\rm j}$	–	<6
Derived transit parameters		
a/R_*	$6.81^{+0.24}_{-0.20}$	$6.93^{+0.11}_{-0.22}$
Stellar density ρ_* [g cm^{-3}]	$0.65^{+0.07}_{-0.05}$	$0.69^{+0.03}_{-0.06}$
Impact parameter b	$0.67^{+0.02}_{-0.03}$	0.648 ± 0.004
Limb-darkening coefficient u_a	0.375 ± 0.026^a	0.36 ± 0.04
Limb-darkening coefficient u_b	0.277 ± 0.015^a	0.24 ± 0.05
Atmospheric parameters of the star		
Effective temperature $T_{\rm eff}$[K]	6041 ± 143	6050 ± 100
Spectroscopic surface gravity $\log g$ [cgs]	4.64 ± 0.13	4.4 ± 0.1
Derived surface gravity $\log g$ [cgs]	4.26 ± 0.05	4.26 ± 0.02
Metallicity [Fe/H] [dex]	0.33 ± 0.11	0.40 ± 0.10
Stellar rotational velocity $V \sin i_*$ [km s^{-1}]	5.5 ± 1.5	5.5 ± 1.5
Spectral type	F8V	F8V
Stellar and planetary physical parameters		
Stellar mass [$M_\odot$]	1.32 ± 0.09	1.27 ± 0.04
Stellar radius [$R_\odot$]	1.42 ± 0.07	$1.38^{+0.05}_{-0.03}$
Planetary mass $M_{\rm p}$ [$M_{\rm Jup}$]	3.23 ± 0.19	3.13 ± 0.10
Planetary radius $R_{\rm p}$ [$R_{\rm Jup}$]	1.20 ± 0.06	$1.16^{+0.04}_{-0.03}$
Planetary density $\rho_{\rm p}$ [g cm^{-3}]	2.33 ± 0.36	$2.49^{+0.16}_{-0.23}$
Planetary surface gravity $\log g_{\rm p}$ [cgs]	3.75 ± 0.04	$3.76^{+0.02}_{-0.03}$
Age t [Gyr]	$2.8^{+1.0}_{-0.8}$	$2.3^{+0.8}_{-0.7}$
Orbital semi-major axis a [au]	0.0449 ± 0.0010	0.0444 ± 0.0005
Equilibrium temperature $T_{\rm eq}$ [K]^b	1637 ± 47	1628 ± 33

Notes. $^{(a)}$ The limb-darkening coefficients were allowed to vary within their 1σ errors related to the uncertainties on stellar atmospheric parameters. $^{(b)}$ Black-body equilibrium temperature assuming a null Bond albedo and uniform heat redistribution to the night side.

Table 5. Kepler-44 system parameters.

Fitted system parameters	Bonomo et al. (2012a)	This work
Orbital period P [days]	3.246740 ± 0.000018	3.2467293 ± 0.0000030
Transit epoch T_0[BJD$_{\rm TDB}$ − 2 454 900]	166.3781 ± 0.0004	287.15640 ± 0.00021
Transit duration T_{14} [h]	3.218 ± 0.043	3.124 ± 0.014
Radius ratio $R_{\rm p}/R_*$	0.0844 ± 0.0011	0.0828 ± 0.0008
Inclination i [deg]	$83.78^{+0.65}_{-0.55}$	$84.96^{+0.50}_{-0.62}$
Limb-darkening coefficient q_1	–	$0.40^{+0.10}_{-0.08}$
Limb-darkening coefficient q_2	–	$0.33^{+0.15}_{-0.13}$
$\sqrt{e}\,\cos\omega$	–	$0.05^{+0.12}_{-0.15}$
$\sqrt{e}\,\sin\omega$	–	0.03 ± 0.20
Orbital eccentricity e	<0.021	<0.066
Radial-velocity semi-amplitude K [m s^{-1}]	124 ± 5	125 ± 11
Systemic velocity $V_{\rm r}$ [km s^{-1}]	-35.892 ± 0.004	-35.892 ± 0.009
RV jitter [m s^{-1}] $s_{\rm j}$	–	<7
Derived transit parameters		
a/R_*	$6.45^{+0.32}_{-0.26}$	$7.07^{+0.35}_{-0.37}$
Stellar density ρ_* [g cm^{-3}]	$0.48^{+0.07}_{-0.06}$	0.63 ± 0.10
Impact parameter b	$0.70^{+0.03}_{-0.04}$	0.62 ± 0.02
Limb-darkening coefficient u_a	0.420 ± 0.026^a	0.42 ± 0.13
Limb-darkening coefficient u_b	0.248 ± 0.017^a	0.21 ± 0.19
Atmospheric parameters of the star		
Effective temperature $T_{\rm eff}$[K]	5757 ± 134	5800 ± 100
Metallicity [Fe/H] [dex]	0.26 ± 0.10	0.15 ± 0.10
Spectroscopic surface gravity $\log g$ [cgs]	4.59 ± 0.14	4.1 ± 0.1
Derived surface gravity $\log g$ [cgs]	4.15 ± 0.06	4.22 ± 0.04
Stellar rotational velocity $V \sin i_*$ [km s^{-1}]	4 ± 2	4 ± 2
Spectral type	G2IV	G2IV
Stellar and planetary physical parameters		
Stellar mass [$M_\odot$]	1.19 ± 0.10	1.12 ± 0.08
Stellar radius [$R_\odot$]	1.52 ± 0.09	1.35 ± 0.08
Planetary mass $M_{\rm p}$ [$M_{\rm Jup}$]	1.02 ± 0.07	1.00 ± 0.10
Planetary radius $R_{\rm p}$ [$R_{\rm Jup}$]	1.24 ± 0.07	1.09 ± 0.07
Planetary density $\rho_{\rm p}$ [g cm^{-3}]	0.65 ± 0.12	$0.93^{+0.19}_{-0.17}$
Planetary surface gravity $\log g_{\rm p}$ [cgs]	3.21 ± 0.05	3.31 ± 0.06
Age t [Gyr]	$6.95^{+1.1}_{-1.7}$	$5.8^{+2.4}_{-1.5}$
Orbital semi-major axis a [au]	0.0455 ± 0.0013	0.0446 ± 0.0011
Equilibrium temperature $T_{\rm eq}$ [K]^b	1603 ± 51	1544 ± 47

Notes. [(a)] The limb-darkening coefficients were allowed to vary within their 1σ errors related to the uncertainties on stellar atmospheric parameters. [(b)] Black-body equilibrium temperature assuming a null Bond albedo and uniform heat redistribution to the night side.

Table 6. Kepler-74 system parameters.

Fitted system parameters	Hébrard et al. (2013)	This work
Orbital period P [days]	7.340718 ± 0.000001	7.340711 ± 0.000006
Transit epoch T_0[BJD$_{\rm TDB}$ − 2 454 900]	67.3453 ± 0.0003	287.56737 ± 0.00014
Transit duration T_{14} [h]	2.699 ± 0.038[a]	3.082 ± 0.011
Radius ratio $R_{\rm p}/R_*$	0.090 ± 0.002	0.0912 ± 0.0009
Inclination i [deg]	85.55 ± 0.96	87.46 ± 0.07
Limb-darkening coefficient q_1	–	$0.36^{+0.10}_{-0.07}$
Limb-darkening coefficient q_2	–	$0.29^{+0.19}_{-0.16}$
Orbital eccentricity e	0.287 ± 0.062	0 (fixed)
Argument of periastron ω [deg]	64 ± 21	–
Radial-velocity semi-amplitude K [m s^{-1}]	58 ± 7	59 ± 11
HARPS-N systemic velocity $V_{\rm r,HN}$ [km s^{-1}]	19.356 ± 0.008	19.366 ± 0.009
HARPS-N RV jitter [m s^{-1}] $s_{\rm j,HN}$	<5	12^{+16}_{-9}
SOPHIE systemic velocity $V_{\rm r,SO}$ [km s^{-1}]	$19.293^{+0.008}_{-0.014}$	19.290 ± 0.014
SOPHIE RV jitter [m s^{-1}] $s_{\rm j,SO}$	28 ± 13	40^{+15}_{-10}
Derived transit parameters		
a/R_*	$11.8^{+1.4}_{-0.8}$	15.47 ± 0.18
Stellar density ρ_* [g cm^{-3}]	$0.58^{+0.22}_{-0.11}$	$1.30^{+0.05}_{-0.04}$
Impact parameter b	0.684 ± 0.032	0.685 ± 0.011
Limb-darkening coefficient u_a	$0.10^{+0.25}_{-0.17}$	0.35 ± 0.17
Limb-darkening coefficient u_b	0.6 ± 0.4	$0.25^{+0.25}_{-0.23}$
Atmospheric parameters of the star		
Effective temperature $T_{\rm eff}$[K]	6050 ± 110	6000 ± 100
Spectroscopic surface gravity log g [cgs]	4.2 ± 0.1	4.5 ± 0.10
Derived surface gravity log g [cgs]	4.2 ± 0.1	4.44 ± 0.01
Metallicity [Fe/H] [dex]	0.34 ± 0.14	0.42 ± 0.11
Stellar rotational velocity $V \sin i_*$ [km s^{-1}]	5.0 ± 1.0	5.0 ± 1.0
Spectral type	F8V	F8V
Stellar and planetary physical parameters		
Stellar mass [$M_\odot$]	$1.40^{+0.14}_{-0.11}$	1.18 ± 0.04
Stellar radius [$R_\odot$]	1.51 ± 0.14	1.12 ± 0.04
Planetary mass $M_{\rm p}$ [$M_{\rm Jup}$]	0.68 ± 0.09	0.63 ± 0.12
Planetary radius $R_{\rm p}$ [$R_{\rm Jup}$]	1.32 ± 0.14	0.96 ± 0.02
Planetary density $\rho_{\rm p}$ [g cm^{-3}]	0.37 ± 0.13	0.88 ± 0.18
Planetary surface gravity log $g_{\rm p}$ [cgs]	2.98 ± 0.11	3.23 ± 0.10
Age t [Gyr]	$2.9^{+1.5}_{-0.8}$	$0.8^{+0.9}_{-0.5}$
Orbital semi-major axis a [au]	0.084 ± 0.014	0.0781 ± 0.0007
Equilibrium temperature $T_{\rm eq}$ [K][b]	1250 ± 120	1078 ± 19

Notes. [(a)] This value of transit duration is not accurate enough because it was estimated with the approximated formula reported in Winn (2010). Indeed, the transit duration is not a free parameter in the transit model adopted by Hébrard et al. (2013). [(b)] Black-body equilibrium temperature assuming a null Bond albedo and uniform heat redistribution to the night side.

Table 7. Kepler-75 system parameters.

Fitted system parameters	Hébrard et al. (2013)	This work
Orbital period P [days]	8.884924 ± 0.000002	8.8849116 ± 0.0000034
Transit epoch T_0[BJD$_{\rm TDB}$ − 2 454 900]	102.9910 ± 0.0002	840.44030 ± 0.00012
Transit duration T_{14} [h]	1.872 ± 0.025[a]	2.0778 ± 0.0084
Radius ratio $R_{\rm p}/R_*$	0.121 ± 0.002	$0.1212^{+0.0009}_{-0.0007}$
Inclination i [deg]	$89.1^{+0.6}_{-1.0}$	$89.12^{+0.51}_{-0.64}$
Limb-darkening coefficient q_1	–	0.36 ± 0.08
Limb-darkening coefficient q_2	–	$0.42^{+0.10}_{-0.08}$
$\sqrt{e}\ \cos\omega$		0.337 ± 0.020
$\sqrt{e}\ \sin\omega$		0.676 ± 0.013
Orbital eccentricity e	0.569 ± 0.010	0.570 ± 0.010
Argument of periastron ω [deg]	63.6 ± 1.4	63.5 ± 1.7
Radial-velocity semi-amplitude K [km s^{-1}]	1.288 ± 0.024	1.287 ± 0.025
HARPS-N systemic velocity $V_{\rm r,HN}$ [km s^{-1}]	−64.175 ± 0.050	−64.180 ± 0.056
HARPS-N RV jitter [m s^{-1}] $s_{\rm j,HN}$	<17	<54
SOPHIE systemic velocity $V_{\rm r,SO}$ [km s^{-1}]	−64.235 ± 0.012	−64.236 ± 0.014
SOPHIE RV jitter [m s^{-1}] $s_{\rm j,SO}$	<8	<8
Derived transit parameters		
a/R_*	19.6 ± 0.6	$19.77^{+0.38}_{-0.45}$
Stellar density ρ_* [g cm^{-3}]	1.79 ± 0.17	$1.85^{+0.11}_{-0.12}$
Impact parameter b	0.14 ± 0.14	$0.13^{+0.09}_{-0.08}$
Limb-darkening coefficient u_a	0.53 ± 0.09	0.50 ± 0.05
Limb-darkening coefficient u_b	0.13 ± 0.26	0.09 ± 0.12
Atmospheric parameters of the star		
Effective temperature $T_{\rm eff}$[K]	5330 ± 120	5200 ± 100
Spectroscopic surface gravity log g [cgs]	4.55 ± 0.14	4.60 ± 0.15
Derived surface gravity log g [cgs]	4.5 ± 0.1	4.50 ± 0.02
Metallicity [Fe/H] [dex]	–0.07 ± 0.15	0.30 ± 0.12
Stellar rotational velocity $V \sin i_*$ [km s^{-1}]	3.5 ± 1.5	3.5 ± 1.5
Spectral type	G8V	K0V
Stellar and planetary physical parameters		
Stellar mass [$M_\odot$]	0.88 ± 0.06	0.91 ± 0.04
Stellar radius [$R_\odot$]	0.88 ± 0.04	0.89 ± 0.02
Planetary mass $M_{\rm p}$ [$M_{\rm Jup}$]	9.9 ± 0.5	10.1 ± 0.4
Planetary radius $R_{\rm p}$ [$R_{\rm Jup}$]	1.03 ± 0.06	1.05 ± 0.03
Planetary density $\rho_{\rm p}$ [g cm^{-3}]	11 ± 2	$11.0^{+0.8}_{-0.9}$
Planetary surface gravity log $g_{\rm p}$ [cgs]	4.36 ± 0.03	4.36 ± 0.03
Age t [Gyr]	6 ± 3	$6.2^{+3.5}_{-2.8}$
Orbital semi-major axis a [au]	0.080 ± 0.005	0.0818 ± 0.0012
Equilibrium temperature at the averaged distance $T_{\rm eq}$ [K][b]	850 ± 40	767 ± 16

Notes. [(a)] This value of transit duration is not accurate enough because it was estimated with the approximated formula reported in Winn (2010). Indeed, the transit duration is not a free parameter in the transit model adopted by Hébrard et al. (2013). [(b)] Black-body equilibrium temperature assuming a null Bond albedo and uniform heat redistribution to the night side.

Table 8. KOI-205 system parameters.

Fitted system parameters	Díaz et al. (2013)	This work
Orbital period P [days]	11.7201248 ± 0.0000021	11.720126 ± 0.000011
Transit epoch T_0[BJD$_{\rm TDB}$ − 2 454 900]	75.17325 ± 0.00012	286.13609 ± 0.00016
Transit duration T_{14} [h]	3.07 ± 0.15	3.069 ± 0.017
Radius ratio $R_{\rm p}/R_*$	0.09849 ± 0.00049	0.09906 ± 0.00094
Inclination i [deg]	88.46 ± 0.05	88.43 ± 0.06
Limb-darkening coefficient q_1	–	$0.45^{+0.12}_{-0.09}$
Limb-darkening coefficient q_2	–	$0.34^{+0.17}_{-0.15}$
$\sqrt{e}\,\cos\omega$	–	0.00 ± 0.05
$\sqrt{e}\,\sin\omega$	–	−0.03 ± 0.010
Orbital eccentricity e	<0.010	<0.015
Radial-velocity semi-amplitude K [km s^{-1}]	3.732 ± 0.039	$3.757^{+0.071}_{-0.084}$
Systemic velocity $V_{\rm r}$ [km s^{-1}]	15.057 ± 0.026	14.922 ± 0.050
RV jitter [m s^{-1}] $s_{\rm j}$	~40	120^{+91}_{-50}
Derived transit parameters		
a/R_*	25.20 ± 0.42	25.07 ± 0.43
Stellar density ρ_* [g cm^{-3}]	2.18 ± 0.10	2.17 ± 0.11
Impact parameter b	0.676 ± 0.014	0.690 ± 0.011
Limb-darkening coefficient u_a	0.523 ± 0.017[a]	0.47 ± 0.17
Limb-darkening coefficient u_b	0.187 ± 0.011[a]	0.21 ± 0.24
Atmospheric parameters of the star		
Effective temperature $T_{\rm eff}$[K]	5237 ± 60	5400 ± 75
Spectroscopic surface gravity log g [cgs]	4.65 ± 0.07	4.7 ± 0.1
Derived surface gravity log g [cgs]	4.550 ± 0.015	4.558 ± 0.014
Metallicity [Fe/H] [dex]	0.14 ± 0.12	0.18 ± 0.12
Stellar rotational velocity $V \sin i_*$ [km s^{-1}]	2.0 ± 1.0	2.0 ± 1.0
Spectral type	K0V	G7V
Stellar and planetary physical parameters		
Stellar mass [$M_\odot$]	0.92 ± 0.03	$0.96^{+0.03}_{-0.04}$
Stellar radius [$R_\odot$]	0.84 ± 0.02	0.87 ± 0.02
BD mass $M_{\rm b}$ [$M_{\rm Jup}$]	39.9 ± 1.0	$40.8^{+1.1}_{-1.5}$
BD radius $R_{\rm b}$ [$R_{\rm Jup}$]	0.81 ± 0.02	0.82 ± 0.02
BD density $\rho_{\rm b}$ [g cm^{-3}]	100.4 ± 6.9	$90.9^{+7.2}_{-6.8}$
Age t [Gyr]	$3.1^{+2.4}_{-1.3}$	$1.7^{+2.5}_{-1.2}$
Orbital semi-major axis a [au]	0.0987 ± 0.0013	0.1010 ± 0.0010

Notes. [(a)] The limb-darkening coefficients were allowed to vary within their 1σ errors related to the uncertainties on stellar atmospheric parameters.